Analysis of stress-induced inhomogeneous electroluminescence in GaN-based green LEDs grown on mesh-patterned Si (111) substrates with n-type AlGaN layer*

Quan-Jiang Lv(吕全江), Yi-Hong Zhang(张一鸿), Chang-Da Zheng(郑畅达)†, Jiang-Dong Gao(高江东), Jian-Li Zhang(张建立), and Jun-Lin Liu(刘军林)

National Institute of LED on Silicon Substrate, Nanchang University, Nanchang 330096, *China*

(Received 7 March 2020; revised manuscript received 7 April 2020; accepted manuscript online 27 May 2020)

Inhomogeneous electroluminescence (EL) of InGaN green LEDs grown on mesh-patterned Si (111) substrate had been investigated. Sample with n-AlGaN inserted between the pre-strained layers and the first quantum well showed the inhomogeneous EL in the low current density range. Near-field EL emission intensity distribution images depicted that inhomogeneity in the form of premature turn-on at the periphery of the LED chip, results in stronger emission intensity at the edges. This premature turn-on effect significantly reduces the luminous efficacy and higher ideality factor value due to locally current crowding effect. Raman measurement and fluorescence microscopy results indicated that the partially relaxed in-plane stress at the edge of the window region acts as a parasitic diode with a smaller energy band gap, which is a source of edge emission. Numerical simulations showd that the tilted triangular n-AlGaN functions like a forward-biased Schottky diode, which not only impedes carrier transport, but also contributes a certain ideality factor.

Keywords: GaN on silicon, edge emission, n-AlGaN, InGaN green LED

PACS: 78.60.Fi, 85.30.–z, 81.05.Ea **DOI:** 10.1088/1674-1056/ab96a2

1. Introduction

Silicon is now widely used as substrates for the epitaxial growth of device quality GaN-based materials. Compared to other substrates technologies, GaN-on-Si technology has greater potential for wafer size scalability and compatibility with silicon integrated circuits processes, which may open up the possibilities of integrating GaN-based LEDs and high electron mobility transistors (HEMTs) for volume production.[1,2] It is well known that III–nitrides have smaller interatomic spacing and thermal expansion coefficients compared to silicon. But like other things, these two properties have their own pros and cons. Recent research has pointed out that the tensile strain caused by the large lattice mismatch can become positive factors for high quality InGaN quantum wells (QWs) with high indium content, which may bring the potential to unlock GaN-based green/yellow LEDs.[3,4] For that to happen, however, appropriate strain management techniques must be employed to avoid high dislocation density and cracks in the device layer due to these two mismatches.

To mitigate film cracking caused by large tensile stress during the film cooling down process, several strain management strategies have been proposed. They are based on two different principles. The first one is the buffer layer technology, which relies on the compressive stress induced by the growth buffer layers to compensate the tensile stress generated upon cooling. These technologies include but are not limited to low-temperature AlN insertion layer,[5] Al(Ga)N/GaN superlattice,[6,7] and the composition grading or step-graded AlGaN buffer layers.[8–10] The second is the selective epitaxy technology, which relies on confining the growth of GaN in small areas and releasing tensile stress by decoupling the GaN layer grown on each mesa to avoid cracking. Selective growth can be performed either by etching the substrate with deep trenches[11] or by patterning the mask mesh.[8,12,13] Nowadays, the successful stress relaxation through the mesh patterned substrates method has made silicon-based GaN-LED commercially available.[14] Some researchers reported that the in-plane stress exhibits a U-shape distribution across the pattern units, the tensile stress is the largest in the middle and relaxes symmetrically towards the square edges.[8,15] Although some edge regions will be removed during the subsequent chip fabrication process, but little was known about the effect of this uneven stress distribution on the optoelectronic performance of the device.

In this article, the inhomogeneous luminescence electroluminescence (EL) at the edge of GaN-based green LEDs grown on mesh-patterned Si (111) substrate was investigated. It is found that this inhomogeneous light emission intensity distribution is caused by the premature turn-on behavior at the periphery of the LED chips. This premature turn-on effect can cause locally overheating and higher ideality factor value due to current crowding, thereby significantly reduce the luminous

*Project supported by the National Key Research and Development Program of China (Grant Nos. 2017YFB0403105 and 2017YFB0403100) and the National Natural Science Foundation of China (Grant Nos. 11674147, 61604066, 51602141, and 11604137).

†Corresponding author. E-mail: zhengchangda@ncu.edu.cn

efficacy in the low current density regimes.

2. Experimental setup

Two green LED samples were grown on 2-inch (1 inch = 2.54 cm) Si (111) substrates by a Thomas Swan close-coupled showerhead metal organic chemical vapor deposition (MOCVD) system. The GaN/InGaN multilayers epitaxially grown on Si (111) with the SiO_2 mesh pattern is shown in Fig. 1(a). The mesh pattern size was kept 1.2 mm×1.2 mm, surrounded by SiO_2 stripes of 5 μm–8 μm in width. The epitaxial structure of sample A consists of following layer in sequence: a 120-nm high temperature AlN buffer layer, a 2.9-μm Si-doped n-GaN, 16 periods InGaN/GaN supperlattices (SLs) grown as strain relief layer and a 16-nm undoped low temperature GaN (LT-GaN). The active region is composed of 4 pairs 2.4-nm thick InGaN QWs, separated by 18-nm thick GaN barrier layer. A 24-nm Mg-doped p-$Al_{0.2}Ga_{0.8}N$ electron blocking layer (EBL) was grown followed by a 220-nm p-GaN: Mg. Finally, the top region of the cladding layer is a 30-nm thick p-GaN layer with heavy Mg-doping to facilitate the formation of Ohmic contact. Sample B has a same epi-structure as sample A expect that the 16-nm-thcik LT-GaN was replaced by a 16-nm-thick n-$Al_{0.2}Ga_{0.8}N$ with 5×10^{17}-cm^{-3} Si-doping.

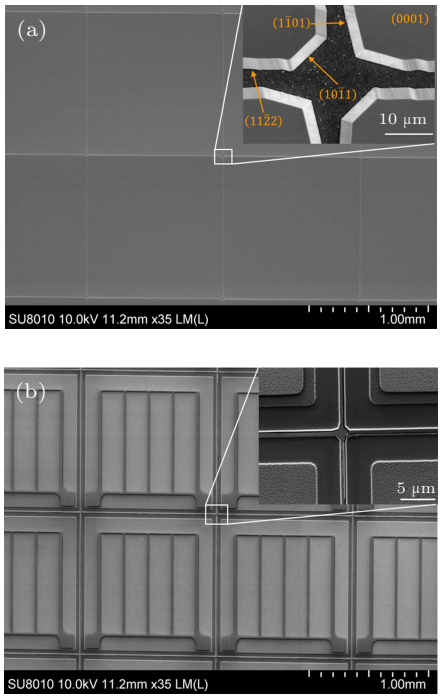

Fig. 1. FE-SEM images of GaN-based LED wafer surface on Si (111) masked with SiO_2 before (a) and after (b) chip process.

The epi-films were processed into vertical LED chips with size of 1.14 mm×1.14 mm, as shown in Fig. 1(b). The GaN film grown near the edge of the patterned unit suffers from stress relaxation due to the freestanding surfaces $(1\bar{1}01)$, $(11\bar{2}2)$, and $(10\bar{1}1)$.[8] To minimize collateral damage and provide access to subsequent chip cutting, we use selective chemical etching to remove all or part of the GaN affected by the edge effect, usually the width is about 70 μm (about 35 μm for each side). Detailed manufacturing process have been reported in our previous works.[14,16] The samples were characterized by the field-emission scanning electron microscope (FE-SEM, Hitachi SU8010) and the fluorescence microscopy (FLM, Nikon C-HGFI with intense 420-490 nm excitation light). Raman spectra were carried out using a Thermo Scientific DXR micro-Raman system to characterize the stress distribution in the epi-film. EL tests were carried out at various currents from 0.01 mA to 750 mA.

3. Results and discussion

Figure 2(a) shows the luminous efficacy as a function of current density (J) at room temperature. Both samples have dominant wavelength of 532 nm at $J = 35$ A·cm^{-2}. The luminous efficacy of the two LEDs increased monotonically from 0.001 A·cm^{-2} onward, reaching a peak value of 320 lm·W^{-1} and 268 lm·W^{-1} at 0.07 A·cm^{-2} and 0.18 A·cm^{-2}, respectively. It can be seen that when J is below 0.75 A·cm^{-2}, sample B having n-AlGaN exhibits lower luminous efficacy than that of sample A; however, as the current density increases, the efficiency of sample B becomes equal or even surpassed that of the sample A. The noticeable luminous efficacy drop of sample B at low current range may be attributed to the apparent increase in defects-induced nonradiative center within the multiple quantum wells (MQWs) caused by the underneath n-AlGaN or some other unpredictable factors. Nevertheless, the inserted n-AlGaN with a higher energy barrier can effectively suppress hole leakage, which may be the reason for the improved luminous efficacy of sample B at high current density regimes.[17]

The semi-logarithmic scale current–voltage (I–V) curves for both samples are shown in Fig. 2(b). The inset is the forward I–V curves plotted in linear scale. The forward voltages of samples A and B at 350 mA were 2.75 V, and 3.11 V, respectively. Besides that, sample B with the n-AlGaN exhibits a higher turn-on voltage and series resistances than that of sample A. This result could be interpreted as the increased effective potential barrier for carriers induced by the insertion of the n-AlGaN.[18,19] In addition, it is worth noting that the leakage current characteristics of sample A is superior to that of sample B in both the low bias region (1.0 V–2.0 V) and the reverse current range. Specifically, the leakage currents for samples A and B at a reverse voltage of −5 V were -2.1×10^{-9} A, and -1.5×10^{-8} A, respectively. Furthermore, it is easy to observe that the slope of the reverse I–V curves has a significant difference between the two samples at low applied reverse bias. The tunneling current in sample A seems to begin

to dominate when the reverse voltage is about 4 V. In contrast, the reverse leakage current in sample B starts to increase abruptly at a reverse voltage of about 2 V. We speculate that the severer field-dependence leakage current of sample B can be attributed to the increased dislocations density as the result of the inserted n-AlGaN.[20] It was already reported that the Shockley–Read–Hall (SRH) nonradiative recombination process induced by crystal defects strongly influences the peak luminous efficacy of LEDs,[21,22] but we believe this should not be the only reason for the significant drop in luminous efficacy of sample B under low injected current density.

In order to clarify the possible association between the inserted n-AlGaN and light emission, near-field emission intensity distribution across the entire LED chip has been detected with current densities of 0.1 A·cm^{-2}, 1.5 A·cm^{-2}, and 7.5 A·cm^{-2} for samples A and B, as illustrated in Fig. 3(a). At $J = 0.1$ A·cm^{-2}, the emission intensity distribution on the entire chip of sample B is extremely uneven compared with sample A. The green emission at the center and red in the peripheral, which means that the light emission is mainly distributed in the peripheral region of the LED chip. This uneven distribution of emission intensity caused by local current crowding can be further quantified by the line profile of the emission intensity at the middle of the latitudinal side of the chip, as indicated by the dashed line in the photographs. However, as the injection current density increases, the emission intensity of the center chip of sample B gradually increases, and eventually becomes equivalent to that of the peripheral region, showing a uniform emission intensity distribution similar to that of sample A.

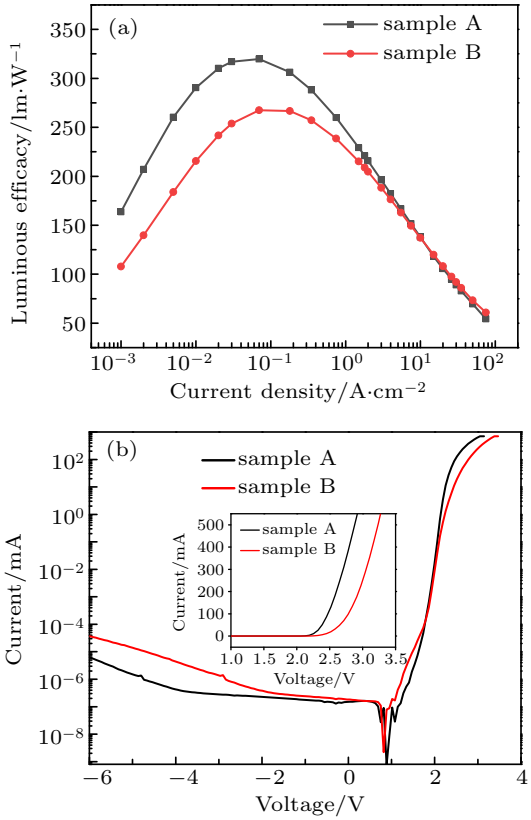

Fig. 2. (a) Experimentally measured luminous efficacy curves *versus* current injection of green LEDs with and without n-AlGaN. (b) Semi-logarithmic scale *I*–*V* characteristics of samples A and B. The inset is the forward *I*–*V* curves of the two LED chips plotted on linear scale.

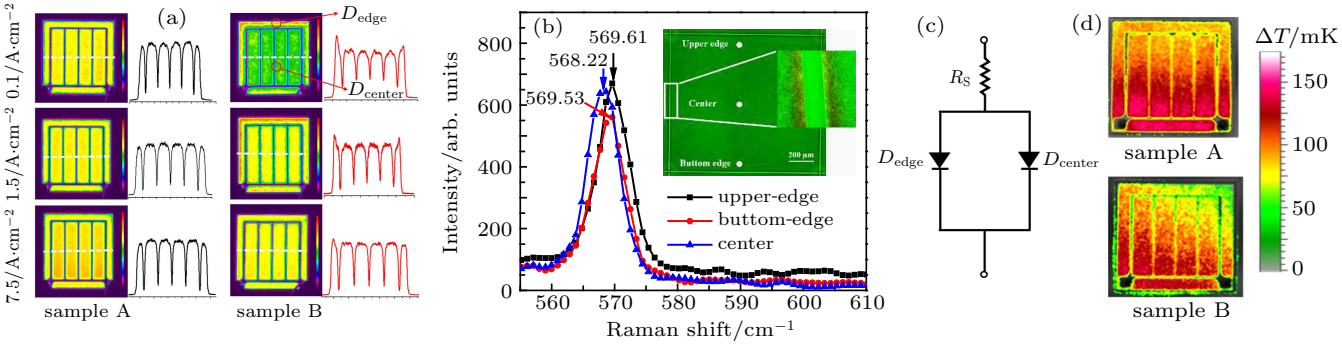

Fig. 3. (a) Near-field emission intensity distribution images of samples A and B at $J = 0.1$ A·cm^{-2}, 1.5 A·cm^{-2}, and 7.5 A·cm^{-2}. The curve to the right of the images represent the light output measured along the dashed line; (b) Micro-Raman spectra collected from edges and center part of the mesh-patterned unit. (c) Schematic diagram of various recombination current components in mesh-patterned LEDs and its corresponding equivalent circuit. (d) Spatial thermal distribution of samples A and B at $J = 0.1$ A·cm^{-2}.

The premature turn-on behavior at the periphery of the LED chips, perhaps related to the specific in-plane stress distribution of the entire epitaxial layer on the patterned substrate compared to the non-patterned substrate. According to Chen *et al.*,[8] the strain is largest at the center of the pattern unit and relaxes symmetrically towards the edges due to the freestanding surface of $(1\bar{1}01)$, $(11\bar{2}2)$, and $(10\bar{1}1)$. To confirm and understand the edge emission, figure 3(b) shows the Raman spectra of the crack-free epi-film at three different positions on the patterned Si (111) with a mesh size of 1.2 mm×1.2 mm. Raman spectra of both samples are similar, so we chose the result of sample A as a representative. A redshift of 1.39 cm^{-1} is observed, translating into a 0.32-GPa less tensile stress at the edge point comparing with the center.[23] Besides, the enlarged FLM near the edge of the pattern unit in the inset shows that the InGaN QWs emit a longer wavelength near the trench. The higher indium content in the QWs may relate to the total amount of freestanding surfaces nearby, as suggested by Zoellner *et al.*[24] Based on this stress-induced difference in indium composition, we divide the chip into two parallel diodes.

The edge region diode (D_{edge}) with a higher indium composition, and the diode locate at the center window region (D_{center}) All the diodes are connected to the series resistance R_s, and the corresponding equivalent circuit is schematically shown in Fig. 3(c). The parallel D_{edge} has a lower energy band gap and smaller area than the main D_{center}. The n-AlGaN inserted in sample B provides an additional energy barrier compared to n-GaN in sample A, causing the parallel D_{edge} of sample B turns on prior to the main D_{center} showing a premature turn-on behavior. The smaller area of the parallel D_{edge} means higher current density at the same injection current levels. Since the luminous efficacy of sample B drops significantly at low current range, there is a reason to believe that the current crowding may be responsible for it. In order to accurately measure spatial heat distribution, sophisticated 60-Hz lock-in thermography was applied to detect the weak source of heat arising at the extremely low current density of 0.1 A·cm^{-2}. As shown in Fig. 3(d), sample A shows a tendency to penetrate evenly from the p-pad to the opposite side. However, the heat distribution of sample B is not so uniform, particularly at the peripheral region of the LED chip where there is local overheating.

The experimental forward *I*–*V* curves and ideality factors are shown in Figs. 4(a) and 4(b), respectively. The corresponding ideality factors are inferred from the slope of a log *I versus V* plot using

$$n_{\text{ideally}} = \frac{q}{kT}\left(\frac{\mathrm{d}\ln I}{\mathrm{d}V}\right)^{-1},$$

where k is the Boltzmann constant, q is the elementary charge, and T is temperature. Both of them depend on the junction current, and three different domains can be clearly distinguished. In the low voltage domain ($V_f \leq 2.0$ V, domain I), the n_{ideally} is high and decreases with increasing current. In this domain, the electrical characteristics of both LED samples are affected by the initial shunt resistance of the p–n junction, which is lower than the junction resistance in the equivalent electrical circuit of LEDs. In the high voltage domain ($V_f > 2.3$ V, domain III), the series resistance clearly dominates and results in an increase in the n_{ideally} with increasing current. It is noteworthy that the Shockley equation, which is well known to describe an ideal diode, only works in the intermediate range ($2.0\ \text{V} < V_f \leq 2.3$ V, linear region of the log *I versus V* plot, domain II). In this domain, the space charge region dominates the device *I*–*V* characteristics and follows a fairly exponential relationship, thus having a local minimum value of the measured ideality factor.[25] In domain II, the ideality factors values of sample B are significantly larger than those of sample A, and also corresponds to the low current density region in Fig. 2(a), where the luminous efficacy of sample B showed a noticeable drop. In addition, in this domain, we observe that the current corresponding to the built-in voltage (the turning point between the linear region and the exponential region in log *I versus V* plot, as indicated by the blue dashed line in Fig. 4(a)) of samples A and B is 10 mA and 0.5 mA, respectively. This distinct correlation shows that the high ideality factor not only data from carrier diffusion and recombination processes; the current crowding effect really makes the ideality factor of sample B larger than sample A. This can also be understood as: the energy barrier is remarkably lower for electrons across n-AlGaN at the peripheral region than the center window region, which leads to the prior turn-on behavior of D_{edge} rather than D_{center}. And the current crowding preferential occurs at the peripheral region as shown in Fig. 3(a).

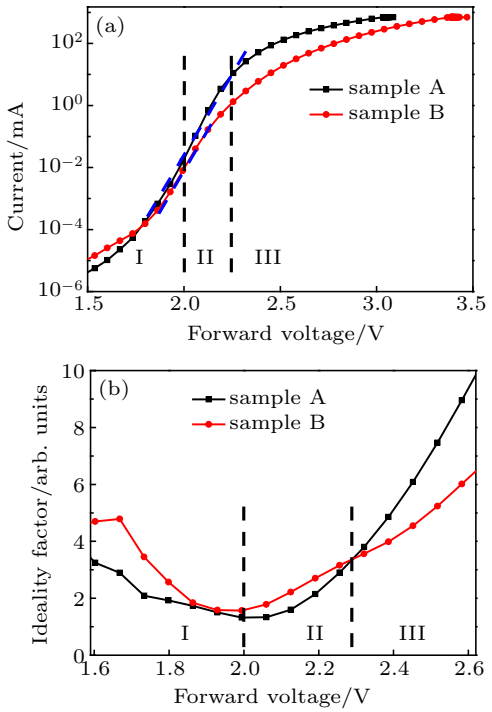

Fig. 4. (a) Semi-logarithmic plot of the forward *I*–*V* characteristics of both samples; (b) Diode-ideality factor extracted from the *I*–*V* analyses *versu* forward bias dependence. Three domains named I, II, and III can be distinguished.

In order to reveal the role of the n-AlGaN on the performance of the ideality factor, numerical simulations of both LED structures with and without n-AlGaN are performed using the Silvaco Atlas modeling software. In the simulation we use the commonly accepted material parameters, and the detailed parameters can be found in our previous work.[26] Figures 5(a) and 5(b) plot the simulated conduction band diagrams (red) and electron concentration distributions (black) in the active region of both samples at 0.1 A·cm^{-2}, respectively. As depicted in Fig. 5(b), after inserting an n-AlGaN, the conduction band near the n-AlGaN shows a large upward tilt from n-GaN to MQWs. The higher effective potential of n-AlGaN can partly block the electrons from injecting into the MQWs. The tilted triangular n-AlGaN functions like a forward biased Schottky diode, which not only impeding carrier transport, but also contributing a certain ideality factor. Besides, due to the spontaneous and piezoelectric polarization sheet charges at the

interfaces between the n-GaN and n-AlGaN, there is a potential minimal region in the conduction band and it is easy to trap electrons result in an electron accumulation.[27] The calculated results are consistent with the decrease in luminous efficacy and the increase in ideality factor at low current density range caused by n-AlGaN. The inserted n-AlGaN changes the transport nature of carriers, which blocks electron injection into the active region and reduces the electron concentration in the MQWs, resulting in a reduced luminous efficacy at low injection current. The correlation between $V_{\rm f}$ and $n_{\rm ideally}$ verifies that larger ideality factor typically results in an increased turn-on and forward voltage.

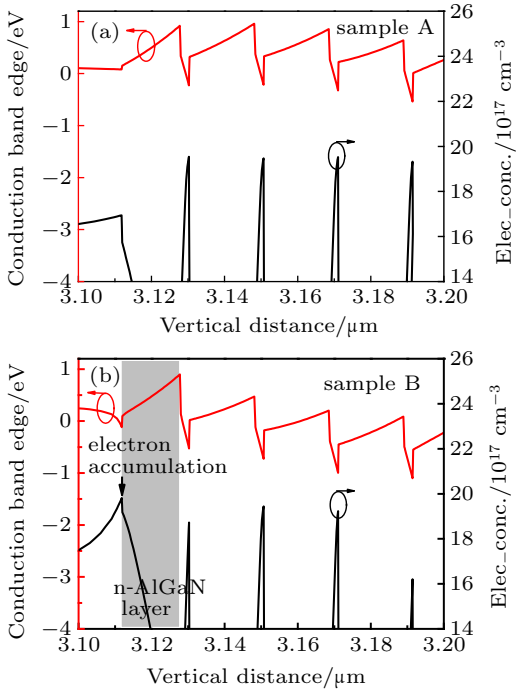

Fig. 5. Simulated conduction band diagrams (red) and electron concentration distributions (black) of InGaN/GaN LEDs without (a) and with (b) n-AlGaN at $J = 0.1$ A·cm^{-2}.

4. Conclusion

In conclusion, we have observed the premature turn-on behavior at the periphery of the LED chips by replacing n-GaN to a higher energy barrier of n-AlGaN between the pre-strained layers and the first QW. For epi-film grown on Si (111) with the SiO_2 mesh pattern, the GaN/InGaN multilayers grown near the edge of the patterned unit suffer from stress relaxation due to the freestanding surfaces $(1\bar{1}01)$, $(11\bar{2}2)$, and $(10\bar{1}1)$. The total amount of independent surfaces makes it easier for indium to be incorporated into the QWs near the edge of chip, resulting in the paralleled diode located at the edge region with a smaller band gap. The inserted n-AlGaN with higher energy barrier can partly block the electrons from injecting into the QWs to induce the edge emission. The premature turn-on behavior at the periphery of the LED chips can cause current crowding effect which in turn leads to local overheating and higher ideality factor values. Therefore, for LEDs grown on mesh-patterned Si (111) substrates, the effect of the premature turn-on behavior should also be considered. The design of the pre-strained layer should avoid an abrupt energy barrier at the interface between the pre-strained layer and the MQWs.

References

[1] Dadgar A 2015 *Phys. Status Solidi* **252** 1063
[2] Chen K J, Haberlen O, Lidow A, Tsai C l, Ueda T, Uemoto Y and Wu Y 2017 *IEEE Trans. Electron Dev.* **64** 779
[3] Jiang F, Zhang J, Xu L, Ding J, Wang G, Wu X, Wang X, Mo C, Quan Z, Guo X, Zheng C, Pan S and Liu J 2019 *Photon. Res.* **7** 144
[4] Liu J L, Zhang J L, Wang G X, Mo C L, Xu L Q, Ding J, Quan Z J, Wang X L, Pan S, Zheng C D, Wu X M, Fang W Q and Jiang F Y 2015 *Chin. Phys. B* **24** 67804
[5] Raghavan S, Weng X, Dickey E and Redwing J M 2005 *Appl. Phys. Lett.* **87** 142101
[6] Feltin E, Beaumont B, Laügt M, De Mierry P, Vennéguès P, Leroux M and Gibart P 2001 *Phys. Status Solidi (a)* **188** 531
[7] Sun Y, Zhou K, Feng M, Li Z, Zhou Y, Sun Q, Liu J, Zhang L, Li D, Sun X, Li D, Zhang S, Ikeda M and Yang H 2018 *Light Sci. Appl.* **7** 13
[8] Chen C H, Yeh C M, Hwang J, Tsai T L, Chiang C H, Chang C S and Chen T P 2005 *J. Appl. Phys.* **98** 093509
[9] Cheng K, Leys M, Degroote S, Van Daele B, Boeykens S, Derluyn J, Germain M, Van Tendeloo G, Engelen J and Borghs G 2006 *J. Electron. Mater.* **35** 592
[10] Lin Y, Zhou S, Wang W, Yang W, Qian H, Wang H, Lin Z, Liu Z, Zhu Y and Li G 2015 *J. Mater. Chem. C* **3** 1484
[11] Zamir S, Meyler B and Salzman J 2001 *Appl. Phys. Lett.* **78** 288
[12] Krost A and Dadgar A 2002 *Materials Science and Engineering B-Solid State Materials for Advanced Technology* **93** 77
[13] Liu J L, Zhang J L, Wang G X, Mo C L, Xu L Q, Ding J, Quan Z J, Wang X L, Pan S, Zheng C D, Wu X M, Fang W Q and Jiang F Y 2015 *Chin. Phys. B* **24** 067804
[14] Jiang F Y, Liu J L, Wang L, Xiong C B, Fang W Q, Mo C L, Tang Y W, Wang G X, Xu L Q, Ding J, Wang X L, Quan Z J, Zhang J L, Zhang M, Pan S and Zheng C D 2015 *Scientia Sinica Physica, Mechanica & Astronomica* **45** 067302
[15] Liu H F, Dolmanan S B, Zhang L, Chua S J, Chi D Z, Heuken M and Tripathy S 2013 *J. Appl. Phys.* **113** 023510
[16] Liu J, Feng F, Zhou Y, Zhang J and Jiang F 2011 *Appl. Phys. Lett.* **99** 111112
[17] Zhang Y, Lv Q, Zheng C, Gao J, Zhang J and Liu J 2019 *Superlattices and Microstructures* **136** 106284
[18] Lin R M, Lai M, Chang L B and Huang C H 2010 *Appl. Phys. Lett.* **97** 181108
[19] Ding B B Z F, Song J J, Xiong J Y, Zheng S W, Zhang Y Y, Xu Y Q, Zhou D T, Yu X P, Zhang H X, Zhang T and Fan G H 2013 *Chin. Phys. B* **22** 088503
[20] Lee M, Lee H U, Song K M and Kim J 2019 *Sci. Rep.* **9** 970
[21] Liu W, Zhao D, Jiang D, Chen P, Liu Z, Zhu J, Li X, Liang F, Liu J, Zhang L, Yang H, Zhang Y and Du G 2016 *J. Phys. D: Appl. Phys.* **49** 145104
[22] Lv Q, Gao J, Tao X, Zhang J, Mo C, Wang X, Zheng C and Liu J 2020 *J. Lumin.* **222** 117186
[23] Tripathy S, Chua S J, Chen P and Miao Z L 2002 *J. Appl. Phys.* **92** 3503
[24] Zoellner M H, Chahine G A, Lahourcade L, Mounir C, Manganelli C L, Schülli T U, Schwarz U T, Zeisel R and Schroeder T 2019 *ACS Appl. Mater. & Inter.* **11** 22834
[25] Zhu D, Xu J, Noemaun A N, Kim J K, Schubert E F, Crawford M H and Koleske D D 2009 *Appl. Phys. Lett.* **94** 081113
[26] Lv Q, Liu J, Mo C, Zhang J, Wu X, Wu Q and Jiang F 2018 *ACS Photon.* **6** 130
[27] Schubert M F, Xu J, Kim J K, Schubert E F, Kim M H, Yoon S, Lee S M, Sone C, Sakong T and Park Y 2008 *Appl. Phys. Lett.* **93** 041102